Preprints of the 21st IFAC World Congress (Virtual)
Berlin, Germany, July 12-17, 2020

Hardware-In-the-Loop Evaluation of a Robust C* Control Law on MuPAL-α Research Aircraft ⋆

R. Takase * **A. Marcos** ** **M. Sato** *** **S. Suzuki** ****

* *Department of Aeronautics and Astronautics, The University of Tokyo, Japan (e-mail: takase-aero@g.ecc.u-tokyo.ac.jp).*
** *Department of Aerospace Engineering, University of Bristol, United Kingdom (Technology for AeroSpace Control (TASC), www.tasc-group.com; e-mail: andres.marcos@bristol.ac.uk).*
*** *Aeronautical Technology Directorate, Japan Aerospace Exploration Agency, Japan (e-mail: sato.masayuki@jaxa.jp).*
**** *Institute of Future Initiatives, The University of Tokyo, Japan (e-mail: tshinji@mail.ecc.u-tokyo.ac.jp).*

Abstract: This article presents the design and evaluation of a robust C* control law through Hardware-In-the-Loop Simulation (HILS) of JAXA's research aircraft called Multi-Purpose Aviation Laboratory (MuPAL-α). The C* control law, which is a widely used flight control architecture in aviation industries, is designed using structured H_∞ synthesis. This design method provides robustness of the controller for flight condition changes and uncertainties associated with the dynamics of MuPAL-α. HILS tests allow on-ground evaluation of controllers using actual actuators. The HILS results show that the designed controller adequately tracks pilot commands in the presence of airspeed variation, uncertainties in the modeling of the onboard actuators, and wind gust.

Keywords: robust control, flight controller, C* control law, Hardware-In-the-Loop Simulation (HILS).

1. INTRODUCTION

In the past few decades, many researchers have applied robust control theory to flight controller design. For example, Dorobantu et al. (2012) designed a flight controller with the H_∞ control framework to obtain robustness for modeling errors. Similarly, robustness against flight condition changes (Hyde (1995)), actuator faults (Liao et al. (2002)), or uncertainties in the modeling of actuator dynamics (Sato and Satoh (2011)) have also been investigated in the community. These studies show that the design of flight controllers must consider flight condition changes and uncertainties associated with aircraft dynamics, and thus their design is tackled via robust control methods.

However, the standard robust control framework has a practical limitation for the flight controller design: the designed controllers have no structural constraints, i.e., the controllers have fully dense state-space matrices with the same order as the generalized plant systems. This property makes it difficult to understand the meaning of the controller matrix coefficients and additional evaluations are needed for the verification and validation process required for aircraft (Shinoda (2014)). In order to smoothly go through this process, industry uses a specific control architecture that is well understood and proven in practice. In addition, it is convenient if the controller's parameters can be tuned through an optimization process that can explicitly include robustness against uncertainties. To meet these requirements, structured H_∞ control design was developed and coded in the MATLAB *hinfstruct* and *systune* commands (Apkarian and Noll (2006); Gahinet and Apkarian (2011); Apkarian et al. (2015)). Recent studies have confirmed the effectiveness of the method for flight control (e.g., Marcos (2017); Biannic and Roos (2018); Marcos and Sato (2017)).

In this article, a C* control law, which is a widely used flight control architecture in the aviation industry (Favre (1994)), is designed using the MATLAB *hinfstruct* command for JAXA's aircraft called Multi-Purpose Aviation Laboratory (MuPAL-α) (Masui and Tsukano (2000)). By using appropriate weighting functions, this design method provides robustness for flight condition changes and uncertainties associated with the dynamics of the actuators. MuPAL-α is a full-scale aircraft equipped with a Fly-by-Wire (FBW) system for testing advanced control methods and has supported both Hardware-In-the-Loop Simulation (HILS) tests and actual flight tests (e.g., Marcos and Sato (2017); Chen et al. (2018); Hardier et al. (2018)). HILS tests allow on-ground evaluation of controllers using actual actuators. The HILS results in this article demonstrated

⋆ This work has received funding from the European Union's Horizon 2020 research and innovation programme under grant agreement No. 690811 and the Japan New Energy and Industrial Technology Development Organization under grant agreement No. 062800, as a part of the EU/Japan joint research project entitled "Validation of Integrated Safety-enhanced Intelligent flight cONtrol (VISION).

the desired robustness (in terms of airspeed changes and actuator uncertainties) of the designed C* control law.

The layout of this article is as follows. Section 2 describes the flight control system. Section 3 describes the controller design method using structured H_∞ synthesis. Section 4 describes the results of the controller analysis and the HILS evaluation, and section 5 ends the article with the conclusions.

2. FLIGHT CONTROL SYSTEM

2.1 Aircraft C control law*

In modern aircraft, pilots control the aircraft with the help of a FBW system (Favre (1994)). Based on the pilot commands and available measured signals, the flight computer calculates the required surface deflections and gives appropriate electronic commands to all actuators. The objectives of the flight control laws integrated with a FBW system are generally to improve the flying qualities of aircraft and to reduce pilot workload.

The longitudinal control law for commercial aircraft is developed, for example, in the form of a feedback controller to satisfy the C* criterion, tracking the vertical load factor command from a pilot (Tobie (1966)). Following Favre (1994), the controller structure used in this article is shown in Fig. 1. The control architecture is composed of the four C* gains. The symbols K_{Nz}, K_{Nzc}, K_{Nzi}, and K_q are the proportional load gain, the feedforward gain, the integral gain, and the pitch rate gain, respectively. Among the C* gains, the load integral gain K_{Nzi} and the proportional gain K_{Nz} mainly affect the load factor performance. The feedforward gain K_{Nzc} affects the closed-loop zeros and the pitch rate gain K_q affects the short-period dynamics. More details about C* gains are discussed in Field (1993).

In Fig. 1, the integral term is needed to improve tracking performance (and in fact, integrators are used in C* control laws in both academia and industry, e.g., Marcos (2017); Favre (1994); Gahinet and Apkarian (2011)). More specifically, a pseudo-integrator $1/(s+\varepsilon)$ is used in order to avoid canceling the zero at the origin of the aircraft dynamics (Gahinet and Apkarian (2011)). The pseudo-integrator is a key point of the controller design in this article, so detailed descriptions are provided in section 3.1.

2.2 Plant Model

The aircraft used in this study is the fixed-wing turboprop research aircraft called MuPAL-α based on a Do228-202 (Fig. 2). The aircraft is equipped with typical control surfaces (a set of ailerons, a single elevator, and a rudder) as well as Direct Lift Control (DLC) flaps. The FBW provides researchers the flexibility of freely designing guidance and control laws, which supports both HILS tests and actual flight tests (Sato and Satoh (2011); Marcos and Sato (2017); Chen et al. (2018)). See Masui and Tsukano (2000) for further details of MuPAL-α and its system architecture.

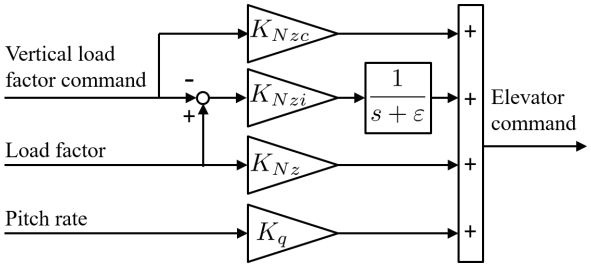

Fig. 1. Longitudinal control law of commercial aircraft.

For the design of the robust C* control law, five independent LTI models of the longitudinal motion are used at different trim conditions based on calibrated airspeed $V_{cas} = \{110,\ 120,\ 130,\ 140,\ 150\}$ kts. This grid corresponds to true airspeed $V_{tas} = \{118,\ 129,\ 140,\ 151,\ 161\}$ kts at an altitude of 5,000 ft under the standard atmospheric condition. The linearized equation of motion is represented as follows:

$$\dot{x}(t) = Ax(t) + B\delta_e(t) \tag{1}$$

where $x(t)$ is the state vector and $\delta_e(t)$ is the elevator deflection (rad). The state vector $x(t)$ is given by

$$x(t) = [\, u(t)\ w(t)\ q(t)\ \theta(t)\,]^T \tag{2}$$

where $u(t)$, $w(t)$, $q(t)$, and $\theta(t)$ are the velocity perturbations in X- and Z- directions (m/s), the pitch rate (rad/s), and the pitch angle (rad), respectively.

The actuator model of MuPAL-α is represented as a first-order system with uncertain time delay:

$$\delta_e = e^{-Ts}\frac{k_a}{T_a s + 1}\delta_{ec} \tag{3}$$

where T_a, k_a, T, and δ_{ec} are respectively the time constant of the modeled first order system, the actuator gain, the uncertain time delay (seconds), and the elevator deflection command (rad). The parameters are $T_a = 0.03$, $k_a = 0.86$, and $T \in [0.06,\ 0.36]$ (seconds). The uncertain time delay captures the uncertainties related to the onboard actuator (Sato and Satoh (2011)). In this article, in order to deal with the uncertainties of the actuator, the following multiplicative perturbation is introduced:

$$e^{-Ts}\frac{k_a}{T_a s+1} = (1 + \underbrace{e^{-Ts}-1}_{\text{perturbation}})\frac{k_a}{T_a s+1} \tag{4}$$

where $e^{-Ts}-1$ is the perturbation and $k_a/(T_a s+1)$ is the delay-free nominal actuator model as in Skogestad and Postlethwaite (1996).

The controller is designed for the plant formed by the 4th order aircraft model (i.e., Eq. (1)) and the 1st order nominal actuator model (i.e., Eq. (3) without $\exp(-Ts)$). Figure 3 shows the pole-zero map of the transfer functions from the elevator deflection command δ_{ec} to the vertical

Fig. 2. Research aircraft MuPAL-α.

load factor N_z with respect to the varying airspeed. From Fig. 3, it is confirmed that the plant has a zero at the origin. This means that pure integral action in the controller is undesirable since it would cancel the zero at $s = 0$ in the system.

One of the focuses of this article is on the influence of the integral term on the designed closed-loop system. This is a fundamental step of controller design since inappropriate selections of controller structures may make the system unstable or will result in situations where the optimization is improperly formulated.

3. CONTROLLER DESIGN

Nonlinearities and uncertainties exist in a wide range of practical systems. In addition, for aircraft its operation environment (e.g. airspeed, air density, etc.) changes during actual flight. In this article, the focus is on robustness against airspeed variations within the ranges typically flown by MuPAL-α. Therefore, the control design objective of this article is to adequately track a command with robustness against:

a) uncertain time delay $T \in [0.06,\ 0.36]$ seconds
b) true airspeed variations from 118 to 161 kts.

3.1 Design Method

The motivation for using structured H_∞ synthesis is as follows. The first is that H_∞ synthesis can help to obtain required robustness against uncertainties by using appropriate weighting functions. The second is that structured H_∞ synthesis, which defines a specific control structure a priori, will facilitate the better understanding of the influence of the individual gains.

Two types of control architecture are investigated: the C* control law using a pure integrator, (e.g. Marcos (2017); Favre (1994)) and the other using a pseudo-integrator, (e.g. Gahinet and Apkarian (2011)). Referring to the integral term in Fig. 1, the following transfer function is defined for the investigation:

$$K_I(s) := \frac{K_{Nzi}}{s+\varepsilon} \tag{5}$$

where ε is the parameter of the integrator. It represents a pure integrator in the case of $\varepsilon = 0$. By using Eq. (5) and the C* gains to be tuned in Fig. 1, the closed-loop

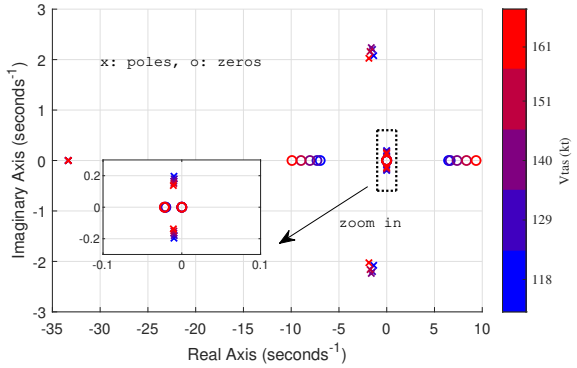

Fig. 3. Pole-zero map of the transfer function from δ_{ec} to N_z.

transfer function from the command $r = N_{zc}$ to the error $e = N_z - N_{zc}$ is given as follows:

$$T_{r2e}(s) = \frac{1 - K_q G_q(s) - G_{Nz}(s)K_{Nz} - G_{Nz}(s)K_{Nzc}}{1 - K_q G_q(s) - G_{Nz}(s)K_{Nz} - G_{Nz}(s)K_I(s)} \tag{6}$$

$$G_{Nz}(s) := \frac{sN_{Nz}(s)}{D(s)}, \quad G_q(s) = \frac{N_q(s)}{D(s)} \tag{7}$$

where $G_{N_z}(s)$ is the transfer function from δ_{ec} to N_z and $G_q(s)$ is the transfer function from δ_{ec} to q. From Eqs. (5) and (6), it can be seen that the main influence on the closed-loop system due to the difference between a pure integrator and a pseudo-integrator is as follows:

- *Pure-integrator ($\varepsilon = 0$)* The response in the low frequency region is given by:

$$\lim_{\omega \to 0} T_{r2e}(j\omega) = \frac{D(0) - N_q(0)K_q}{D(0) - N_q(0)K_q - N_{Nz}(0)K_{Nzi}} \quad (\varepsilon = 0) \tag{8}$$

where ω is the frequency of the system. Equation (8) means that the sensitivity function in low frequency regions can be shaped to improve control performance by tuning the gains K_{Nzi} and K_q.

However, the transfer function $G_{N_z}(s)$ has a zero at the origin so the controller $K_I(s)$ cancels the zero at $s = 0$ in the sensitivity function $T_{r2e}(s)$. This is undesirable since the system is marginally stable.

- *Pseudo-integrator ($\varepsilon \neq 0$)* The response in the low frequency regions is given by:

$$\lim_{\omega \to 0} T_{r2e}(j\omega) = 1 \quad (\varepsilon \neq 0) \tag{9}$$

which means that the sensitivity function in low frequency regions cannot be improved to be smaller than 1 (i.e., 0 dB). Note that the difference from the pure integrator arises from avoiding the pole/zero cancellation in the term of Eq. (10) taken from Eq. (6) as shown below.

$$G_{Nz}(s)K_I(s) = \frac{sK_{Nzi}N_{Nz}(s)}{(s+\varepsilon)D(s)} \quad (\varepsilon \neq 0) \tag{10}$$

For any practical applications, including the HILS tests, it is recommended that a robust C* control law uses the pseudo-integrator to prevent the system from becoming marginally stable. Therefore, the design scheme proposed in this article is as follows.

In the controller design phase, we have to use only a pure integrator to avoid the performance limitation from Eq. (9). This is a compromise such that the C* gains can be obtained with improved performance (even in low frequency regions) by using weighting functions in terms of H_∞ requirements. After obtaining the C* gains, the pure-integrator is replaced by the pseudo-integrator, and then an a-posteriori analysis is performed for the controller with the pseudo-integrator to confirm control performance.

3.2 Design Result

Similarly to Sato (2018), the following weighting function W_u is selected to cover the gains of $e^{-Ts} - 1$ with the

maximum time delay $T = 0.36$ seconds so that the crossover frequency is as high as possible.

$$W_u = \frac{3.5s}{s+9} \tag{11}$$

Subsequently, the weighting function W_e is introduced for the output $e = N_z - N_{zc}$ to impose a tracking requirement for the vertical load factor command from the pilot. Figure 4 shows the block diagram for the design of the C* control law with structured H_∞ controller. Regarding the two scalar uncertainties $\mathrm{diag}(\Delta_e, \Delta_u)$, the symbols Δ_e and Δ_u are respectively the uncertainty blocks for the tracking performance and the actuator uncertainty.

The following weighting function W_e is selected heuristically to ensure adequate tracking performance.

$$W_e = \frac{k_1 s + k_2}{k_3 s + 1} \tag{12}$$

Among the three tuning parameters, k_1 and k_2 are fixed first since they mainly affect the control performance in the case of the C* control law (see also the resulting sensitivity function, i.e. transfer function from r to e in Fig. 5). From this figure it is seen that the sensitivity has a relatively high constant gain in the frequency region below 10^{-2} rad/s. The high constant gain in the low frequency derives from the structure of the controller as shown Eq. (8). If we seek high tracking performance, the peak of the sensitivity also becomes large due to the waterbed effect, resulting in large overshoot. Therefore, the value of k_2 is set to be as large as possible while maintaining an acceptable overshoot. Then, k_1 is fixed and k_3 is determined to satisfy $\gamma < 1$, where γ is the H_∞ norm of the closed-loop system.

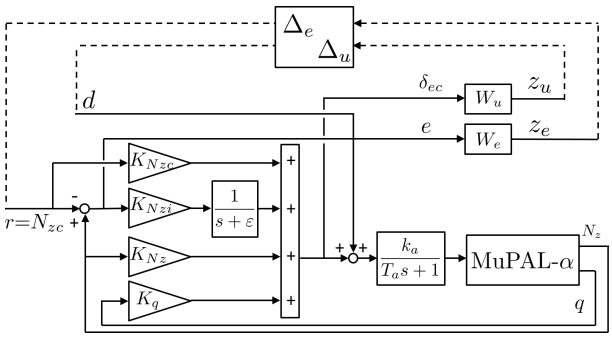

Fig. 4. Block diagram for the design of the C* control law.

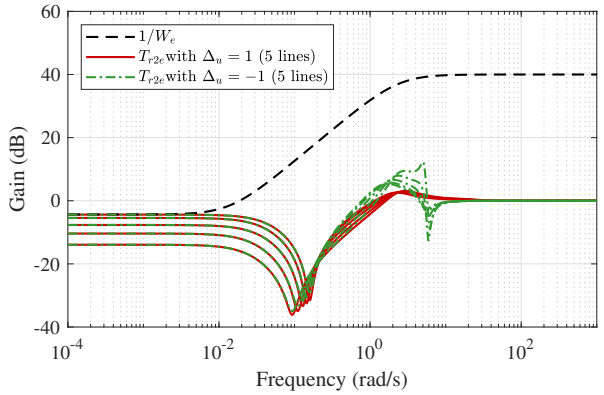

Fig. 5. Design result: Gain plot of sensitivity functions with the controller using the pure integrator.

According to this procedure, the tuning parameters $k_1 = 0.7$, $k_2 = 1.65$ and $k_3 = 70$ are selected.

For the consideration of the flight condition changes, the multiple model approach (Ackermann (1985)) is used so that a set of common C* gains are designed for the 5 plant models with $V_{tas} = \{118,\ 129,\ 140,\ 151,\ 161\}$ kts. By using the above mentioned weighting functions, the MATLAB *hinfstruct* command gives the structured H_∞ controller after several iterations with six random initial gains. Figure 5 shows the sensitivity functions with the designed gains for $\Delta_u = 1$ (solid red line) and $\Delta_u = -1$ (dashed green line) respectively for each of the 5 plants. Note that the closed-loop system for $\Delta_u = 1$ corresponds to the controlled MuPAL-α for the maximum supposed delay $T = 0.36$ seconds. As seen in Fig. 5, the controller satisfies the controller design requirements.

4. CONTROLLER ANALYSIS AND EVALUATION

4.1 A-Posteriori Analysis

For the HILS tests, the designed controller is discretized via a zero-order hold at a sampling period of the onboard computer of MuPAL-α $T_z = 0.02$ seconds. As noted in section 3.1, the pure-integrator is replaced by the pseudo-integrator. Thus, an a-posteriori analysis is performed for the controller implemented with the pseudo-integrator. Afterwards, the flight controller is evaluated through HILS tests on MuPAL-α.

The parameter of the pseudo-integrator is set to $\varepsilon = 0.021$ ($\varepsilon > T_z$). Figure 6 shows the gain plots when the pure integrator is replaced by the pseudo-integrator. It is observed that the original desired performance W_e is not fully achieved since the gain plots is above $1/W_e$ for low frequency regions. However, this is a known side-effect of using a pseudo-integrator as shown in Eq. (9) (and a necessary compromise in order to guarantee sufficient stability margin). As a part of the a-posteriori analysis, the compromised performance is investigated. The controller (replaced by the pseudo-integrator) would satisfy performance with any value of $k_2 < 1$, for example $\hat{W}_e(k_2 = 0.9)$, which is depicted in Fig. 6 with a dotted blue line for reference. It should be noted that $\hat{W}_e$ ($k_2 = 0.9$) is only depicted so as to show the control performance check which is conducted a posteriori. More specifically, although

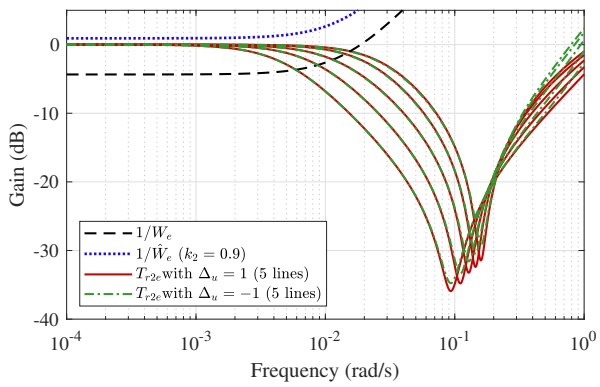

Fig. 6. A-posteriori analysis: Gain plot of sensitivity functions with the controller, in which the pure integrator is replaced by the pseudo-integrator.

the gains of the sensitivity functions are exactly 0 dB at $\omega = 0$ rad/s, the gains in between 10^{-4} and 10^{-2} rad/s are below 0 dB (e.g., the gains are below -0.004 dB at 10^{-3} rad/s).

Figure 7 shows the time-domain responses of the controller for the true airspeed cases of $V_{tas} = \{118, 129, 140, 151, 161\}$ kts. The simulation is carried out in MATLAB/Simulink environment around the trim condition. The simulation model is composed of Eqs. (1) and (3) with time delays $T = 0.06$ and 0.36 seconds (the minimum and maximum values of the range). The upper figure shows the vertical load factor N_z (m/s^2) and the lower one shows the commanded input δ_{ec} (deg). The black dashed line shows the reference command. The solid lines show the behavior when the time delay $T = 0.06$ seconds and the dash-dot lines when $T = 0.36$ seconds. The controller adequately tracks the command. Therefore, the controller has robustness for time delays and flight condition changes.

To summarize the a-posteriori analysis, adequate control performance has been shown in the numerical simulation environment. For evaluating robustness against uncertainties in the behavior of the actual actuator dynamics, HILS tests are carried out and shown in the next subsection.

4.2 Hardware-In-the-Loop Simulation

HILS tests for MuPAL-α were performed on 26^{th} June 2019 inside the airplane hangar at JAXA in Tokyo, Japan. In the tests, the FBW computer is connected to the emulation computer. The control surfaces are controlled and actually moved by pilot commands. Then, the actual positions of the control surfaces are obtained as inputs to the simulation by the emulation computer (Masui and Tsukano (2000)). For the HILS tests, the designed controller is implemented in C-code.

Four evaluation tests were performed: combining with/without gust conditions with two initial airspeeds. The two initial airspeeds (V_{tas}={120, 140} kts) are selected to investigate the robustness of the flight controller at low and high speed within the range of operation typically flown by MuPAL-α. During the HILS tests, the load factor command N_{zc} is created by deflecting the column in the cockpit. The command is provided by a pilot who produces a doublet command shape in order to keep the true airspeed within the operating range.

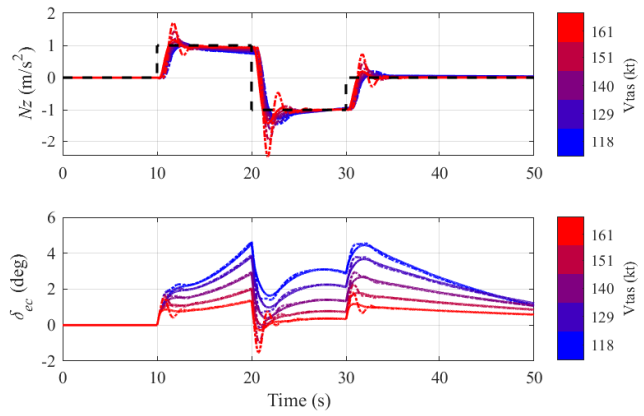

Fig. 7. Time-domain responses of the controller replaced by the pseudo-integrator.

Figure 8 shows the result of the HILS test in the case of the initial airspeed $V_{tas} = 120$ kt without wind gusts. The figure shows, from top to bottom, the true airspeed (TAS, kt), the deviation of the X-directional airspeed u_a (m/s), the Z-directional airspeed w_a (m/s), the pitch rate q (m/s^2), the set of the vertical load factor command N_{zc} and the vertical load factor N_z (m/s^2), and the set of the elevator deflection command δ_{ec} and the elevator deflection δ_e (deg), respectively. From the top plot, it is seen that the true airspeed is changed starting around 120 kt up to 140 kt due to the pilot command. The designed controller adequately tracks the command under the airspeed variation and the uncertainties of the actuator.

Figure 9 shows the result of the HILS test in the case of the initial airspeed around $V_{tas} = 140$ kt with wind gusts. The plot layout is the same as in Fig. 8 except for the second and the third plots which include the X-and Z-directional wind gusts in solid blue lines. The robust C* control law shows adequate tracking performance even in the presence of wind gust.

5. CONCLUSION

This article has presented the design and evaluation of a robust C* control law for the fixed-wing research aircraft MuPAL-α. The proposed design scheme can provide a controller including a pseudo-integrator (to avoid pole/zero cancellation) while providing flexibility in the gain tuning phases of the structured H_∞ controller design. In order to evaluate robustness against uncertainties, Hardware-In-the-Loop Simulation (HILS) tests have been carried out for the designed controller. The results show that the controller adequately tracks the pilot's load factor commands in the presence of the airspeed variation and uncertainties arising from actual actuator dynamics.

ACKNOWLEDGEMENTS

The authors would like to thank Mr. Hosoya for his assistance in the HILS test and Dr. Waitman for the expert knowledge regarding structured H_∞ controller design.

REFERENCES

Ackermann, J. (1985). Multi-model approaches to robust control system design. In *Uncertainty and Control*, 108–130. Springer.

Apkarian, P., Dao, M.N., and Noll, D. (2015). Parametric robust structured control design. *IEEE Transactions on Automatic Control*, 60(7), 1857–1869.

Apkarian, P. and Noll, D. (2006). Nonsmooth H_∞ Synthesis. *IEEE Transactions on Automatic Control*, 51(1), 71–86.

Biannic, J.M. and Roos, C. (2018). Robust Autoland Design by Multi-Model H_∞ Synthesis with a Focus on the Flare Phase. *Aerospace*, 5(1), No. 18.

Chen, L., Alwi, H., Edwards, C., and Sato, M. (2018). Evaluation of a Sliding Mode Fault Tolerant Controller on the MuPAL-α Research Aircraft. In *2018 IEEE Conference on Control Technology and Applications (CCTA)*, 760–765. IEEE.

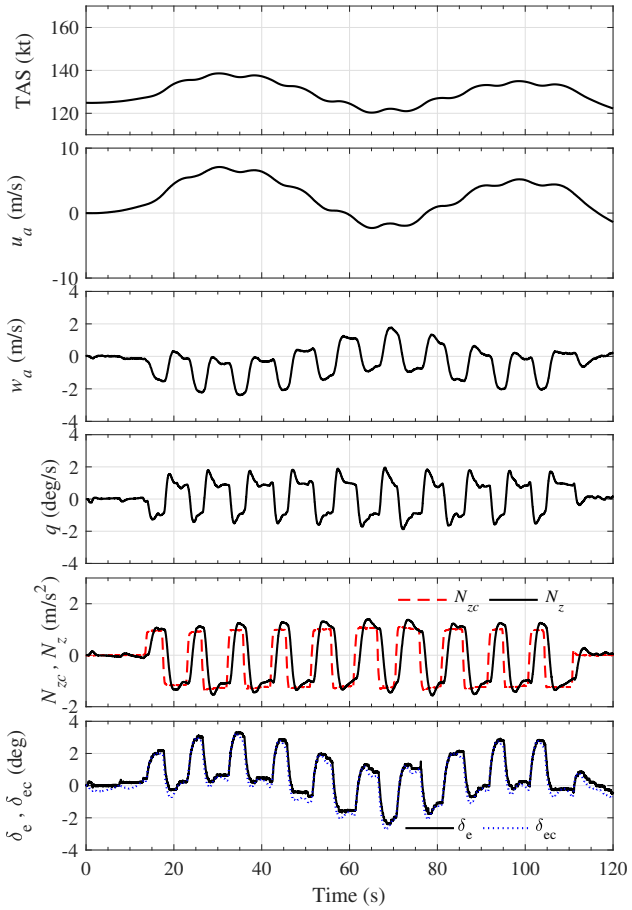

Fig. 8. The HILS result in the case of the initial airspeed around $V_{tas} = 120$ kt without wind gusts.

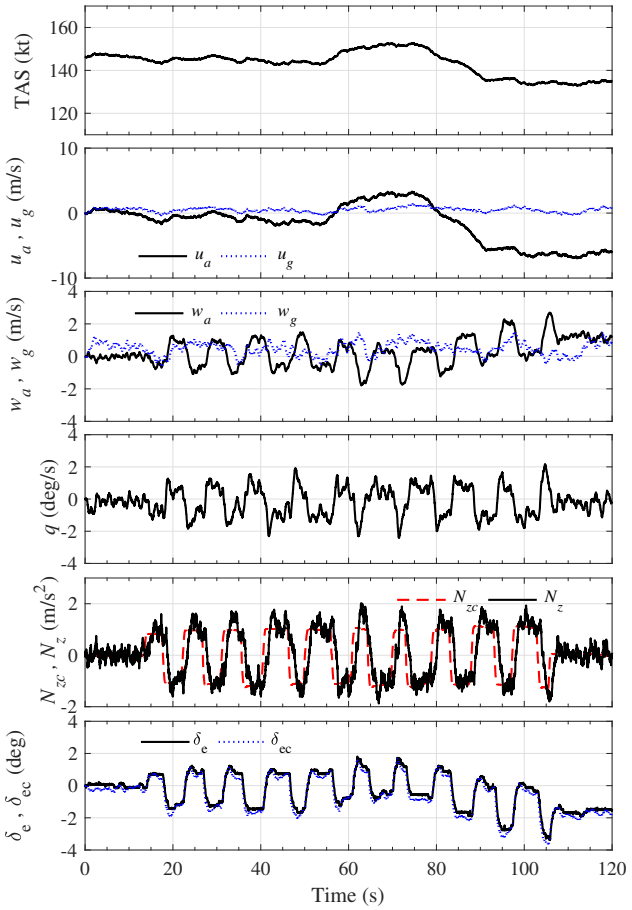

Fig. 9. The HILS result in the case of the initial airspeed around $V_{tas} = 140$ kt with wind gusts.

Dorobantu, A., Murch, A., and Balas, G. (2012). H_∞ robust control design for the NASA AirSTAR flight test vehicle. In *50th AIAA Aerospace Sciences Meeting including the New Horizons Forum and Aerospace Exposition*, AIAA 2012–1181.

Favre, C. (1994). Fly-by-wire for commercial aircraft: the Airbus experience. *International Journal of Control*, 59(1), 139–157.

Field, E. (1993). The application of a C* flight control law to large civil transport aircraft. Cranfield College of Aeronautics Report No 9303.

Gahinet, P. and Apkarian, P. (2011). Structured H_∞ Synthesis in MATLAB. In *IFAC, 2011 Proceedings of*, 1435–1440. IFAC.

Hardier, G., Ferreres, G., and Sato, M. (2018). Design and flight testing of an adaptive gain-scheduled controller using on-line model estimation. In *2018 IEEE Conference on Control Technology and Applications (CCTA)*, 766–773. IEEE.

Hyde, R. (1995). *H_∞ Aerospace Control Design*. Springer-Verlag London Ltd.

Liao, F., Wang, J.L., and Yang, G.H. (2002). Reliable robust flight tracking control: an LMI approach. *IEEE Transactions on Control Systems Technology*, 10(1), 76–89.

Marcos, A. (2017). Revisiting the aircraft C* control law: A comparison between classical and structured H-infinity designs. In *2017 IEEE Conference on Control Technology and Applications (CCTA)*, 2114–2119. IEEE.

Marcos, A. and Sato, M. (2017). Flight testing of an structured H-infinity controller: An EU-Japan collaborative experience. In *Control Technology and Applications (CCTA), 2017 IEEE Conference on*, 2132–2137. IEEE.

Masui, K. and Tsukano, Y. (2000). Development of a new in-flight simulator mupal-alpha. In *Modeling and Simulation Technologies Conference*, AIAA 2000–4574.

Sato, M. (2018). Gain-scheduled flight controller using bounded inexact scheduling parameters. *IEEE Transactions on Control Systems Technology*, 26(3), 1074–1082.

Sato, M. and Satoh, A. (2011). Flight Control Experiment of Multipurpose-Aviation-Laboratory-α In-Flight Simulator. *Journal of Guidance, Control, and Dynamics*, 34(4), 1081–1096.

Shinoda, K. (2014). Process of Safety and Development Assurance for Commercial Aircraft- Application for the MRJ Development (in Japanese). In *11th Workshop Of Critical Software*.

Skogestad, S. and Postlethwaite, I. (1996). *Multivariable feedback control: analysis and design*. John Wiley & Sons, Inc.

Tobie, H.N. (1966). A new longitudinal handling qualities criterion. In *Proc. 18th Annual National Aerospace Electronics Conference*, 93–99.